

# Seam-guided local alignment and stitching for large parallax images

Tianli Liao<sup>1,2\*</sup>, Chenyang Zhao<sup>1,2</sup>, Lei Li<sup>1,2</sup>, Heling Cao<sup>1,2</sup>

<sup>1</sup>College of Information Science and Engineering, Henan University of Technology, Henan, China.

<sup>2</sup>Key Laboratory of Grain Information Processing and Control (Henan University of Technology), Ministry of Education, Henan, China.

\*Corresponding author(s). E-mail(s): [tianli.liao@haut.edu.cn](mailto:tianli.liao@haut.edu.cn);

Contributing authors: [zhaochy2005@163.com](mailto:zhaochy2005@163.com); [leili@haut.edu.cn](mailto:leili@haut.edu.cn); [caohl@haut.edu.cn](mailto:caohl@haut.edu.cn);

## Abstract

Seam-cutting methods have been proven effective in the composition step of image stitching, especially for images with parallax. However, the effectiveness of seam-cutting usually depends on that images can be roughly aligned such that there exists a local region where a plausible seam can be found. For images with large parallax, current alignment methods often fall short of expectations. In this paper, we propose a local alignment and stitching method guided by seam quality evaluation. First, we use existing image alignment and seam-cutting methods to calculate an initial seam, and evaluate the quality of pixels along the seam. Then, for pixels with low qualities, we separate their enclosing patches in the aligned images and locally align them by extracting modified dense correspondences via SIFT flow. Finally, we composite the aligned patches via seam-cutting and merge them into the original aligned result to generate the final mosaic. Experiments show that compared with the state-of-the-art seam-cutting methods, our result is more plausible and with fewer artifacts. The code will be available at <https://github.com/tlliao/Seam-guided-local-alignment>

**Keywords:** Image stitching, Seam-cutting, Quality evaluation, Local alignment, SIFT flow

## 1 Introduction

Image stitching has been well-studied for decades in computer vision [23], which mainly involves image alignment [3, 7, 9, 12, 14, 15, 19, 25, 28–31], composition and blending [4, 13, 22]. In consumer-level photography, parallax is the most intractable issue due to the unconstrained shooting environment. Existing alignment methods may still fail to handle it. Therefore, it is usually the image composition that determines the quality of the final stitching result.

Seam-cutting and seam-driven approaches [5, 10, 16–18, 26], which aim to find an optimal seam in the overlapping region from one or finite alignment candidates, have been proven effective in handling parallax. However, as a second step after image alignment in image stitching, the effectiveness highly depends on the alignment accuracy. It means that the images should at least be roughly aligned such that there exists a local region where a plausible seam can be found. For images with large parallax, existing alignment methods may fail to align them locally (see Fig. 1(b)), resulting

in the seam-cutting failing to produce plausible results (see Fig. 1(c,d)).

In this paper, we propose a local alignment and stitching method to handle the misaligned artifacts that occur in the seam-cutting results. Specifically, we first utilize existing alignment and seam-cutting methods to produce a rough stitching result. Second, a seam quality evaluation is performed to find the “problematic” pixels, which guides us to separate their enclosing patches in the pre-aligned results. Then, we extract the dense correspondences between the patches and smoothly align them via the modified SIFT flow. Finally, we use seam-cutting to composite the aligned patches and merge them into the former rough result. Experiments show that compared with the state-of-the-art seam-cutting [16, 17] or seam-driven methods [18, 26], our method can produce results with fewer artifacts and overall, more visually pleasing.

Our method has two major contributions.

- We propose a novel seam-cutting method by locally aligning the misaligned pixels along the initial seam and recalculating a new seam. It can almost remove the assumption that the images should be roughly aligned.
- Our pipeline can be integrated with any advanced alignment techniques, and the local alignment strategy can be applied to any seam-cutting method.

## 2 Related Work

We briefly review the approaches most related to our work. A comprehensive survey of image stitching algorithms is given in [23].

### 2.1 Seam-cutting Methods

The seam-cutting approach is a powerful and widely used composition method [1, 10, 11, 16, 17, 27], which is usually expressed in terms of energy minimization and minimize it via graph-cut optimization [2]. Agarwala *et al.* [1] applied seam-cutting to generate “digital photomontage”, they defined the energy function as the sum of a data penalty selecting by the user and an interaction penalty involving the colors, gradients, and edges of an image.

Zhang *et al.* [27] combined alignment error and color difference in the energy function to find a

better seam that avoids splitting misaligned pixels with similar colors. Li and Liao [16] considered the nonlinearity and nonuniformity of human perception into seam-cutting and defined a sigmoid-metric color difference and saliency weights in the energy function. To avoid objects from being cropped, omitted, or duplicated, Herrmann *et al.* [10] utilized object detection to match objects between images, and introduced three new terms to the traditional energy function that address the above issues, respectively. Liao *et al.* [17] indicated that the seam with minimal cost is not necessarily optimal in terms of human perception. Then, they proposed an iterative seam estimation method where a quality evaluation algorithm for pixels along the seam is designed to guide the iteration procedure.

### 2.2 Seam-driven Methods

The seam-driven strategy was first proposed by Gao *et al.* [8]. They indicated that the perceptually best result is not necessarily from the best global alignment. Thus, they generated finite alignment candidates from multiple RANSAC [6] procedures and applied seam-cutting to estimate multiple seams from these candidates. Then, a seam quality metric is defined to evaluate these seams and the seam with minimal cost is chosen to produce a final mosaic. Zhang and Liu [26] improved the screening process of alignment candidates by combining homography with content-preserving warps. They used the seam cost of the energy function to evaluate the seam quality. Lin *et al.* [18] generated the alignment candidates via a superpixel-based feature grouping and a structure-preserving warp. The warp is gradually improved via adaptive feature weighting. They also defined a seam quality metric based on the zero-mean normalized cross-correlation (ZNCC) score.

In both seam-cutting and seam-driven methods, their main focus is to find an optimal seam from the pre-aligned images, which are settled before generating the final mosaic. For images with large parallax, these methods may easily fail if the alignment methods fail to locally align the images. Our method, on the other hand, aligns the local regions in pre-aligned images until a high-quality seam is found.

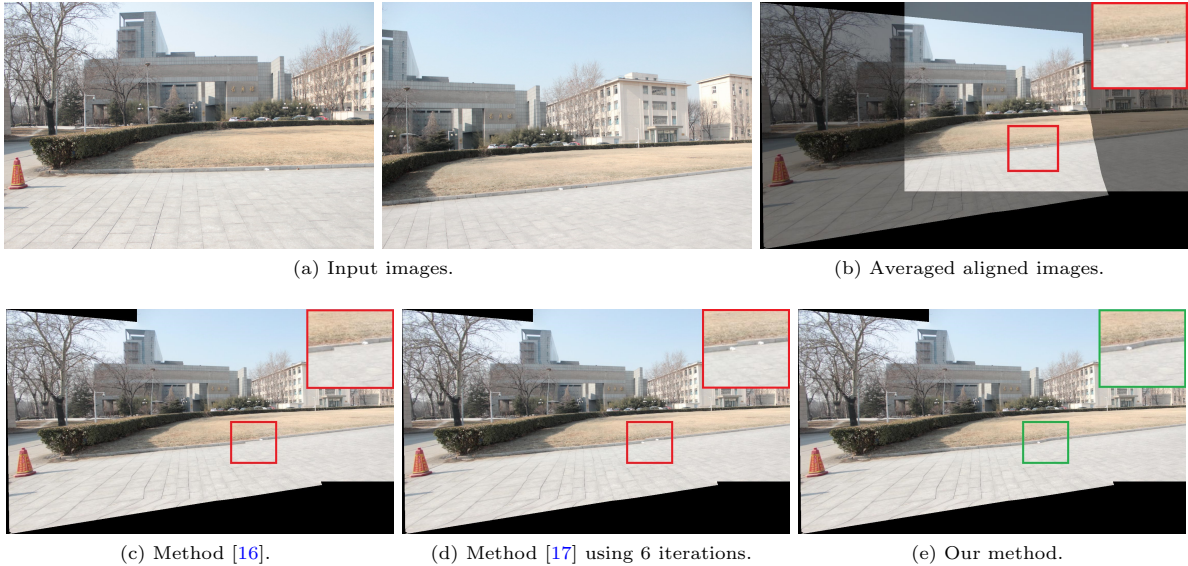


**Fig. 1:** Result comparisons with state-of-the-art seam-cutting methods. Aligned images are obtained via method [15]. (b) Aligned images with overlapping region averaged. See that the curbs are totally misaligned.

### 3 Method

In this section, we first briefly describe the conventional seam-cutting. Then, we give a comprehensive description of our method, including SSIM-based seam evaluation, misaligned components extraction, local patch alignment, and seam merging.

In the following, we use  $I_0$  and  $I_1$  to denote the aligned target and reference images, which can be generated via any advanced alignment method.  $P_i$  ( $i = 0, 1$ ) denotes a local patch in the overlapping region in  $I_0$  and  $I_1$ , respectively.

#### 3.1 Conventional Seam-cutting

Let  $\mathcal{O}$  denote the overlapping region of  $I_0$  and  $I_1$ , and  $\mathcal{L} = \{0, 1\}$  be a label set, where “0” and “1” correspond to  $I_0$  and  $I_1$ , respectively. Then a seam means assigning a label  $l_p$  to each pixel  $p \in \mathcal{O}$ . The goal of the seam-cutting method is to find a labeling  $l$  that minimizes the energy function

$$E(l) = \sum_{p \in \mathcal{O}} D_p(l_p) + \sum_{(p,q) \in N} S_{p,q}(l_p, l_q) \quad (1)$$

where the data penalty  $D_p$  measures the cost of assigning a label  $l_p$  to pixel  $p$ , the smoothness

penalty  $S_{p,q}$  measures the cost of assigning a pair of labels  $(l_p, l_q)$  to a pair of neighboring pixels  $(p, q) \in N$ .

#### 3.2 SSIM-based Seam Evaluation

After aligning the input images, we first calculate an initial seam  $S_0$  via the seam-cutting method. Then, similar to [17], we use the structural similarity (SSIM) index [24] to evaluate each pixel  $p_i$  on the seam. We extract two local patches  $P_0$  and  $P_1$  centered at  $p_i$ , and define the evaluation error for  $p_i$  as

$$Q(p_i) = \mathcal{D} \left( \frac{1 - \text{SSIM}(P_0(p_i), P_1(p_i))}{2} \right) \quad (2)$$

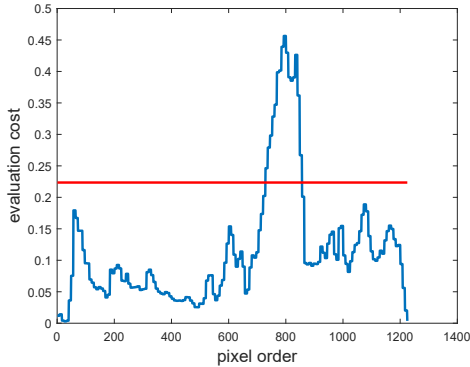
where  $\mathcal{D}$  is a denoising operator same as [17], which is adopted to alleviate the effect of small misalignments (invisible to human eyes). Fig. 2(a) illustrates the seam evaluation for seam  $S_0$ , pixels with high errors usually mean misaligned parts.

#### 3.3 Components Extraction

Thanks to the advanced alignment methods, the initial seam usually just partially fails, even for images with large parallax. Our goal is to “repair”



(a) Seam-cutting result via [16]



(b) Evaluation errors.

**Fig. 2:** SSIM-based seam evaluation. (a) The seam is shown as a hot map based on the evaluation errors. (b) Evaluation errors of seam  $S_0$  that is shown as a 1-D signal with threshold  $\tau = 0.2235$ .

these failed parts. As mentioned in [17], a plausible seam should have a relatively small error  $Q$  for any pixel. Thus, for pixels with high errors, we separate them in the seam for subsequent alignment as follows,

- if  $\max(Q) \leq k\text{mean}(Q)$ , we consider  $S_0$  as a plausible seam;
- else, we calculate a threshold  $\tau$  via Ostu’s method [21], and consider  $p_i$  with  $Q(p_i) \geq \tau$  as misaligned.

The threshold  $\tau$  splits the seam into several components (see Fig. 2(b)). It’s worth noting that the threshold may not be precise enough to identify misaligned pixels. We tolerate some false positives since the subsequent alignment process does not lead to worse results. For each misaligned component  $C_i$ , we separate its enclosing rectangular patches  $\mathcal{P}_0^i, \mathcal{P}_1^i$  in corresponding aligned images, respectively. Fig. 3(a,b) shows an example of how the patches are separated in  $I_0$  and  $I_1$ .

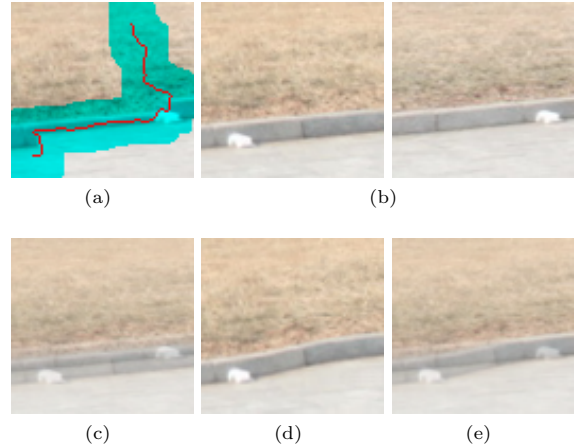


**Fig. 3:** Components extraction and alignment for misaligned pixels. (a) Separated rectangular patch with identified misaligned pixels marked in red. Cyan region represents the extracted patches in the seam evaluation for these pixels. (b) Separated patches  $\mathcal{P}_0, \mathcal{P}_1$  in  $I_0$  and  $I_1$ , respectively. (c) Result of average blending for (b). (d) Aligned patch  $\mathcal{P}_0$ . (e) Result of average blending for aligned  $\mathcal{P}_0$  and  $\mathcal{P}_1$ .

### 3.4 Patch Alignment

The separated patches are pre-aligned, but with structure misalignment (see Fig. 3(c)), we consider there exists no or only a small parallax between these patches. Thus, we can construct the dense correspondences via SIFT flow [20] between pixels in the patches. Theoretically, for each pixel  $p_j$  in  $\mathcal{P}_0^i$ , there exists a shift vector  $V^i(p_j)$  that satisfies

$$\|\mathcal{P}_0^i(p_j + V^i(p_j)) - \mathcal{P}_1^i(p_j)\| = 0 \quad (3)$$

Then, we can align the two patches via vector flow  $V^i$ . However, if the boundary pixels of the patch  $\mathcal{P}_0^i$  have big shift vectors, merging the aligned patches into pre-aligned results will introduce more artifacts around the patch, see Fig. 4 for an example. We smoothly modify the vector flow as  $f(V^i(p_j))$  where  $f$  is a sigmoid function

$$f(t) = \frac{1}{1 + e^{-\beta(t-0.5)}} \quad (4)$$

For horizontal patch alignment,  $t$  is the x-coordinate of the pixel in patch  $\mathcal{P}_0^i$ , which is normalized to  $[0, 1]$ .  $\beta$  controls the rate of change

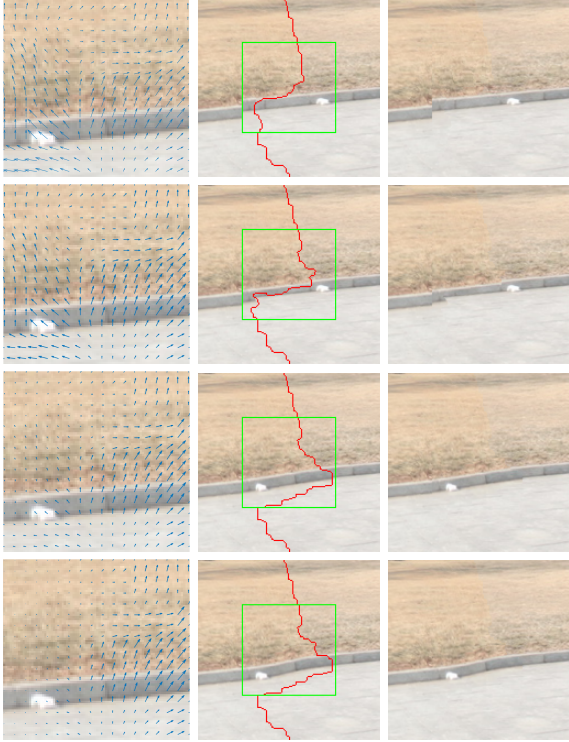


**Fig. 4:** Illustration for patch alignment and seam merging process. From **left to right**: vector flow, local seam-cutting result and local composited result. We only show the part of the vector flow for clarity. From **top to bottom**: the result of original  $V^i$ , modified  $f(V^i)$  with  $\beta = 1, 4, 8$  in Eq. (4), respectively. The **green** rectangle in the second column represents the position of the separated patch. Note that the third column only shows the simple composited results without gradient domain fusion.

for  $f$ . The sigmoid function makes the aligned patches smoothly consistent with  $I_0$  at  $t = 0$ , and smoothly consistent with  $I_1$  at  $t = 1$ . Fig. 4 shows the modified vector flow under different settings of  $\beta$ .

### 3.5 Seam Merging

Due to the modification for vector flow, the separate patches are just partially aligned, see Fig. 3(d,e) for an example. We still need the seam-cutting method to composite the patches. Note that the local seam  $s_i$  in the aligned patches must be connected with the initial seam  $S_0$  end to end. Otherwise, artifacts may occur at the junction of

the two seams. To avoid introducing new artifacts, we constrain the local seam to be connected with the initial seam by finding a label  $l^i$  in which the data penalty for pixel  $p_j \in \mathcal{P}_0^i$  is

- $D_{p_j}(0) = 0, D_{p_j}(1) = \infty$ , if  $p_j \in \partial\mathcal{P}_0^i$  with  $l_{p_j} = 0$  in the initial seam  $S_0$ ;
- $D_{p_j}(0) = \infty, D_{p_j}(1) = 0$ , if  $p_j \in \partial\mathcal{P}_0^i$  with  $l_{p_j} = 1$  in the initial seam  $S_0$ ;
- $D_{p_j}(0) = 0, D_{p_j}(1) = 0$ , otherwise,

where  $\infty$  is set to avoid mislabeling,  $\partial\mathcal{P}_0^i$  represents the border of  $\mathcal{P}_0^i$ . Fig. 4 shows an example including seam merging process. We can see that the local seam is accurately merged with initial seam.

We summarize our method in Algorithm 1.

---

**Algorithm 1** Seam-guided local alignment and stitching.

---

**Require:** two aligned images  $I_0$  and  $I_1$ ;

**Ensure:** a final stitching seam  $S_*$ ;

- 1: calculate an initial seam-cutting result  $S_0$  via method [16];
  - 2: evaluate the pixels along the seam via SSIM-based seam evaluation in Eq. (2);
  - 3: identify whether there are misaligned pixels along the seam;
  - 4: **if** misaligned pixels exist **then**
  - 5:     extract misaligned components  $\{\mathcal{C}_i\}_{i=1}^n$  in seam  $S_0$  based on threshold  $\tau$ ;
  - 6:     **for** each  $\mathcal{C}_i$  **do**
  - 7:         separate the enclosing patches  $\mathcal{P}_0^i$  and  $\mathcal{P}_1^i$  from  $I_0$  and  $I_1$ , respectively;
  - 8:         estimate the SIFT flow [20] between  $\mathcal{P}_0^i$  and  $\mathcal{P}_1^i$  and obtain the flow vector  $V_i$ ;
  - 9:         modify the flow vector via the sigmoid function  $f$  in Eq. (4);
  - 10:         align  $\mathcal{P}_0^i$  and  $\mathcal{P}_1^i$  via  $f(V_i)$ ;
  - 11:         calculate a local stitching seam  $s_i$  in the two aligned patches;
  - 12:         obtain a new seam  $S_i$  by merging  $s_i$  into the last seam in the corresponding position.
  - 13:     **end for**
  - 14: **end if**
  - 15: **return**  $S_* = S_n$
-

## 4 Experiments

In our experiments, the patch size for seam evaluation is set to be  $21 \times 21$ ,  $k$  in Sec. 3.3 equals 1.5,  $\beta$  equals 8. Input images are aligned via [15], the initial seam is calculated via [16]. Our method is then adopted to align the local patches and improve the initial seam, and the final result is generated by blending the aligned images via gradient domain fusion [22]. We compare our method with two seam-cutting methods [16, 17], the seam-cutting results are generated using their open codes with default settings. We also test our method on public image datasets [18, 26].

### 4.1 Quantitative Comparison

Since the evaluation error in Eq. (2) can represent the quality of a stitching seam to some extent, we use it to quantitatively evaluate our method. For the stitching seam  $S$ , we define the quality error as

$$e(S) = \frac{1}{N} \sum_{i=1}^N \frac{1 - \text{SSIM}(P_0(p_i), P_1(p_i))}{2} \quad (5)$$

where  $p_i$  is the pixel on the seam,  $N$  is the total number of the pixels on the seam. A smaller value usually indicates a better seam and a more convincing stitching result. We test these methods on three image datasets, including 20 image pairs from our dataset, 35 image pairs from [26] and 24 image pairs from [18]. Fig. 5 illustrates the 20 image pairs of our dataset.

Fig. 6 shows the quantitative comparison results between our method and the other two seam-cutting methods. Our method achieves the lowest errors in most cases and has the best stitching quality. We show parts of the results with significantly visual improved seam quality in Fig. 7, where the seams are shown as hot maps based on the quality errors. Note that the quality error of our method is a bit bigger than method [17] for No. 17. image pairs in SEAGULL dataset, while our visual result is much better (see the dinosaur’s back leg). This may be because the average for the seam quality will miss the differences between the “good” and “bad” pixels. We leave the more precise quality evaluation for stitching seam as a future work.

We also compare the computational efficiency with the other seam-cutting methods. We run these methods on the three image datasets. All the experiments are run in the same environment with a 3.4GHz Intel Core i7 CPU and a 32GB memory. Fig. 8 shows the elapsed time of the tested methods on three datasets. The recorded time only includes seam-cutting, where the image alignment process is not taken into account. It’s obvious that the method [16] is most efficient as it only calculates one stitching seam. Our method takes a little more but acceptable time as it involves SIFT flow calculation, patch alignment and seam merging. Method [17] takes too much time in some cases since it iterates dozens of times to find a better seam, as shown in Fig. 9.

We also specifically record the iteration number in method [17] and the number of extracted patches in our method, which may be the main factor that affects the elapsed time, as shown in Fig. 9. It is observed that the iteration numbers of different image pairs are quite different, and the elapsed time of method [17] is approximately proportional to the iteration number, while the number of patches are relatively stable, and the increasing number of patches does not necessarily result in more elapsed time, the resolutions of the patches may have a greater effect on the elapsed time.

### 4.2 Results Comparison

We compare our method with methods involving seam-cutting algorithms, including photomerge<sup>1</sup> in Photoshop, Microsoft ICE<sup>2</sup>, [16, 17] and seam-driven methods [18, 26]. Since the codes of the two seam-driven methods are publicly unavailable, we also test our method on their shared datasets.

Fig. 10 demonstrates a challenging example in [26]. Obvious parallax can be seen from the buildings and the ground. Input images and the results of [26] are from the website<sup>3</sup>. Microsoft ICE fails to produce a plausible result. Photomerge, methods [16] and [17] all fail in the ground, see the red rectangle marked in the results. Method

---

<sup>1</sup><https://helpx.adobe.com/photoshop/using/create-panoramic-images-photomerge.html>

<sup>2</sup><https://www.microsoft.com/en-us/research/project/image-composite-editor>

<sup>3</sup><http://web.cecs.pdx.edu/~fliu/project/stitch/>



Fig. 5: Our image dataset for quantitative comparison.

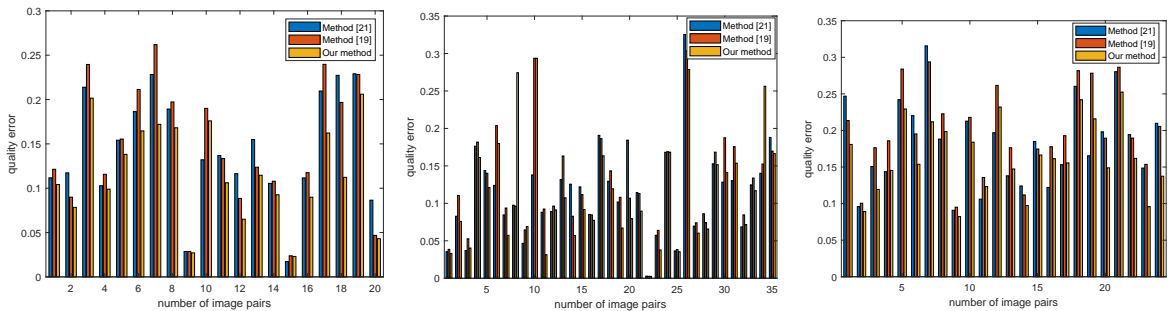


Fig. 6: Quantitative comparisons on different image datasets. From left to right: our dataset, dataset from [26] and dataset from SEAGULL [18].

[26] and SEAGULL [18] have small artifacts introduced by seam-cutting (see marked regions in red rectangles). Overall, our result is more plausible.

Fig. 11 shows another example tested in our dataset. Photomerge fails to produce any result. Microsoft ICE suffers from severe artifacts. Both [16] and [17] fail to produce pleasing results due to the misaligned stairs. By locally aligning these stairs and merging them with other parts, our method can generate a plausible mosaic. Note that the difference between the two stitching seams in Fig. 11(d,e) is actually very small. Thus, it is indeed the alignment process that improves the seam-cutting method.

### 4.3 User-study

In order to investigate whether our proposed method improves the perceived image quality, we manually selected image pairs with controversial seam-cutting results, and conduct a user study to compare with the other two seam-cutting methods. We invite 20 participants to rank the selected 8 unannotated groups of stitching results based on which looks best and artifacts-free. Then, we record the score by assigning weights 4, 2 and 1 to Rank 1, 2 and 3. Table 1 shows a summary of rank votes and total scores for three methods, which demonstrates that our stitching results win most users' favor.

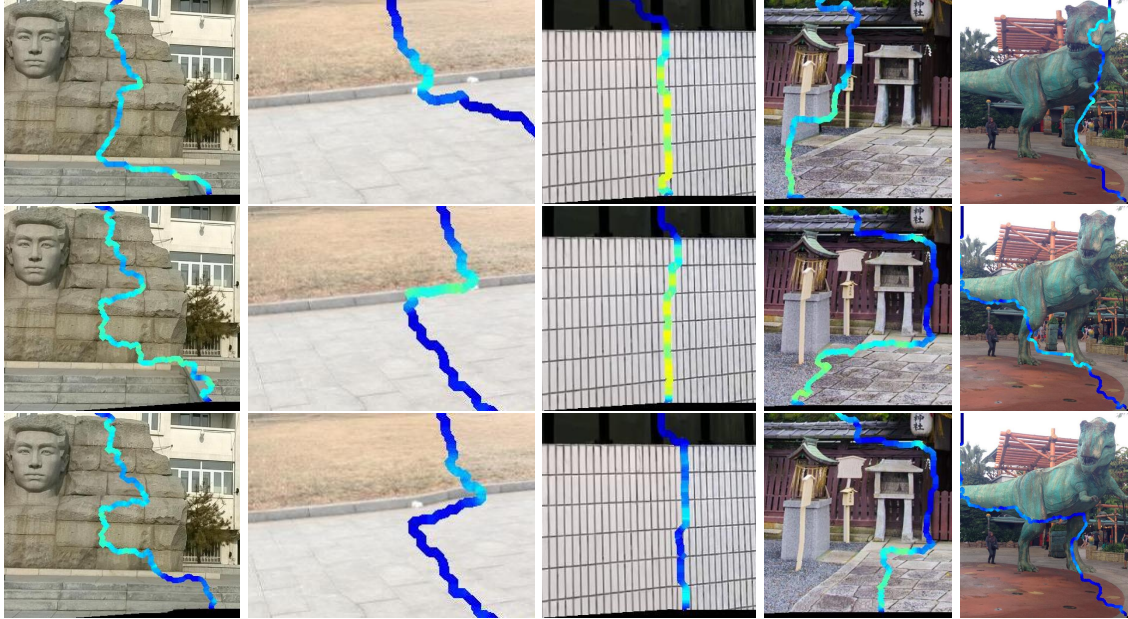


**Fig. 7:** Seam-cutting comparison with the other two seam-cutting methods. Seams are shown as hot maps. From top to bottom: method [17], method [16] and ours. From left to right: No. 3,4,18 from our dataset, No. 26 from dataset [26], No. 17 from SEAGULL dataset [18].

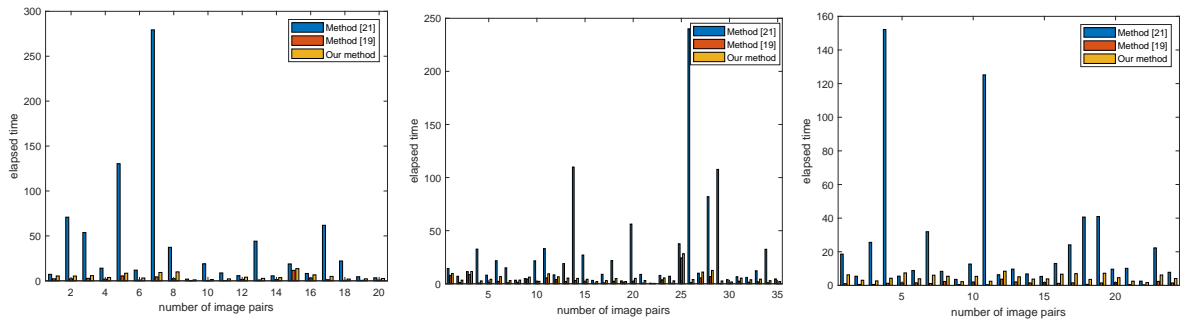


**Fig. 8:** Comparison of the elapsed time with the other two seam-cutting methods. From left to right: our dataset, dataset from [26] and dataset from SEAGULL [18].

**Table 1:** Score results of user study.

Methods	Results			
	Rank 1	Rank 2	Rank 3	Total score
Method [17]	16	59	84	266
Method [16]	36	71	54	340
Ours	108	30	22	514

#### 4.4 Limitations

Seam-cutting methods have the assumption that images can be roughly aligned such that there exists a local region where a plausible seam can be found. Our method takes a step forward in removing this assumption, however, it still has limitations. We assume that the existing seam-cutting result is only partially problematic. If misaligned pixels occur throughout the seam, our method may need to align the entire overlapping region via SIFT flow, which is hardly probable for images with large parallax. Besides, the local

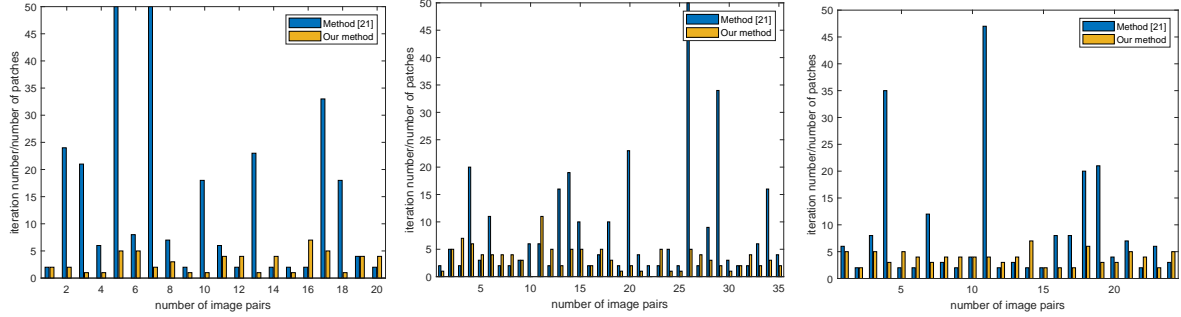


**Fig. 9:** Specific comparison on factors that affect the elapsed time. Y label represents the iteration numbers in [17] or the number of extracted patches in our method. From left to right: our dataset, dataset from [26] and dataset from SEAGULL [18].

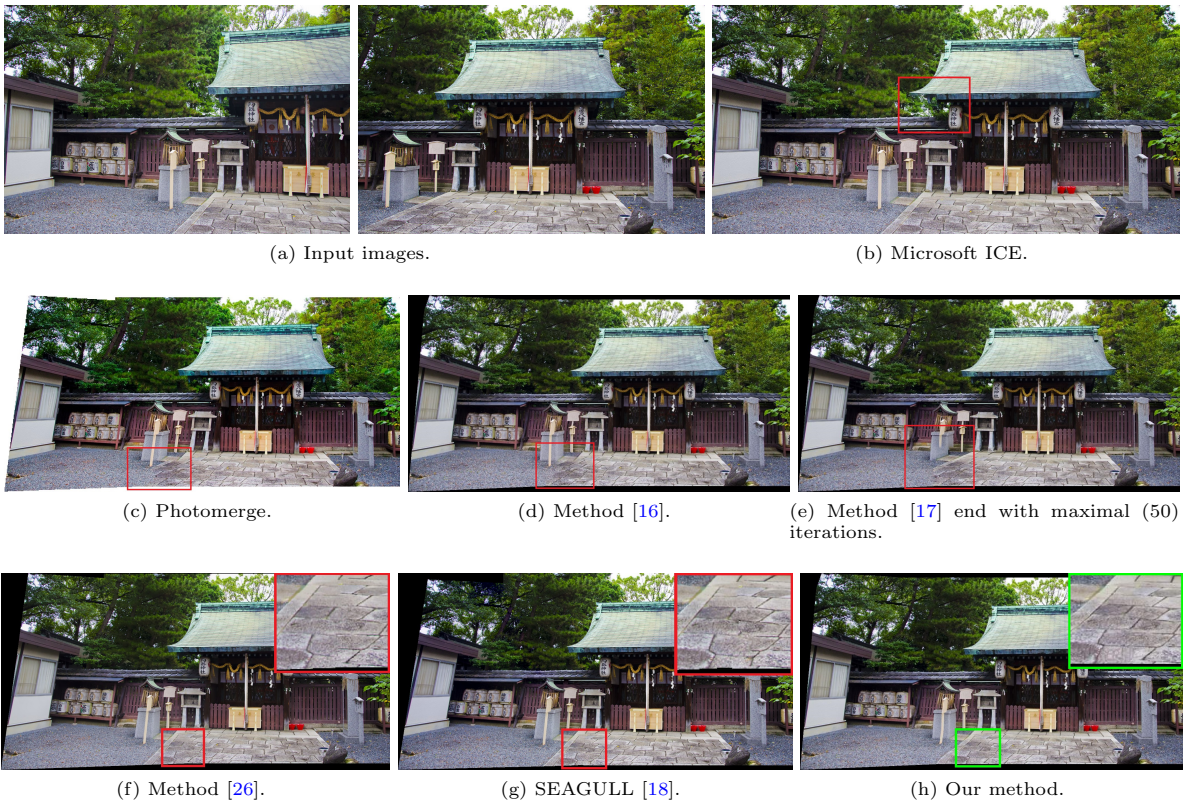


**Fig. 10:** Results comparison with other seam-cutting and seam-driven methods. (Best to zoom-in and view on screen).

alignment usually works for structure misalignments near the seam. Fig. 12 shows a failure example in [9], method [15] could not align the numbers, which results in a big displacement that our method cannot repair it either. We leave it as our future work.

## 5 Conclusion

In this paper, we propose a seam-guided local alignment and stitching method to handle the images with large parallax. We first applied image alignment and seam-cutting methods to obtain an



(a) Input images.

(b) Microsoft ICE



(c) Method [17] with 21 iterations and seam-cutting result.



(d) Method [16] and seam-cutting result.

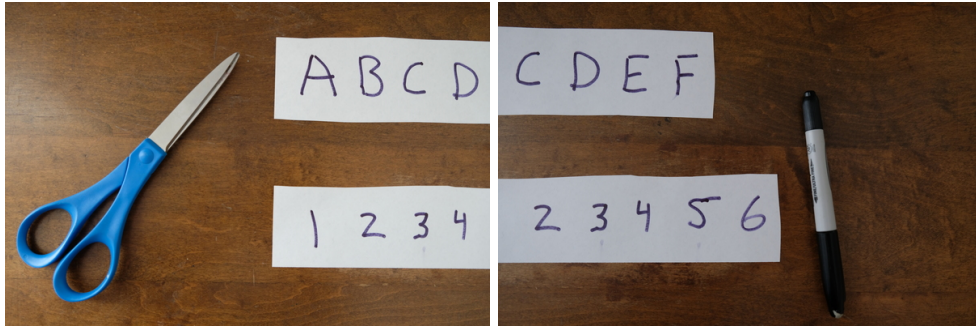


(e) Our method.

**Fig. 11:** Results comparison with other seam-cutting methods. We also show the corresponding seam-cutting results (Best to zoom-in and view on screen).

initial seam. Then, we evaluate the pixels along the seam and extract misaligned components of the seam. For each component, we separate its enclosing rectangular patches in pre-aligned

images and estimate modified dense correspondence via SIFT flow, which is utilized to align the patches. Finally, we calculate a local seam and merge it into the initial seam. Experiments on



(a) Input images.



(b) Method [16] and seam-cutting result.



(c) Our method.

**Fig. 12:** Failure Example.

the different datasets show the superiority of our method.

## References

- [1] Agarwala A, Dontcheva M, Agrawala M, et al (2004) Interactive digital photomontage. *ACM Trans Graph* 23(3):294–302
- [2] Boykov Y, Veksler O, Zabih R (Nov. 2001) Fast approximate energy minimization via graph cuts. *IEEE Trans Pattern Anal Mach Intell* 23(11):1222–1239
- [3] Brown M, Lowe DG (2007) Automatic panoramic image stitching using invariant features. *Int J Comput Vis* 74(1):59–73
- [4] Burt PJ, Adelson EH (1983) A multiresolution spline with application to image mosaics. *ACM Transactions on Graphics* 2(4):217–236
- [5] Dai Q, Fang F, Li J, et al (2021) Edge-guided composition network for image stitching. *Pattern Recognition* 118:108019
- [6] Fischler MA, Bolles RC (1981) Random sample consensus: a paradigm for model fitting with applications to image analysis and automated cartography. *Commun ACM* 24(6):381–395
- [7] Gao J, Kim SJ, Brown MS (2011) Constructing image panoramas using dual-homography warping. In: *Proc. IEEE Conf. Comput. Vis. Pattern Recognit.*, pp 49–56
- [8] Gao J, Li Y, Chin TJ, et al (2013) Seam-driven image stitching. *Eurographics* pp 45–48
- [9] Herrmann C, Wang C, Bowen RS, et al (2018) Robust image stitching with multiple registrations. In: *Proceedings of the European*

- Conference on Computer Vision (ECCV), pp 53–67
- [10] Herrmann C, Wang C, Strong Bowen R, et al (2018) Object-centered image stitching. In: Proc. 15th Eur. Conf. Comput. Vision, pp 821–835
- [11] Kwatra V, Schödl A, Essa I, et al (2003) Graphcut textures: image and video synthesis using graph cuts. *ACM Trans Graph* 22(3):277–286
- [12] Lee KY, Sim JY (2020) Warping residual based image stitching for large parallax. In: Proceedings of the IEEE/CVF Conference on Computer Vision and Pattern Recognition (CVPR)
- [13] Levin A, Zomet A, Peleg S, et al (2004) Seamless image stitching in the gradient domain. In: Proc. 8th Eur. Conf. Comput. Vision, pp 377–389
- [14] Li J, Wang Z, Lai S, et al (2018) Parallax-tolerant image stitching based on robust elastic warping. *IEEE Trans Multimedia* 20(7):1672–1687
- [15] Li J, Deng B, Tang R, et al (2019) Local-adaptive image alignment based on triangular facet approximation. *IEEE Transactions on Image Processing* 29:2356–2369
- [16] Li N, Liao T, Wang C (2018) Perception-based seam cutting for image stitching. *Signal, Image and Video Processing* 12(5):967–974
- [17] Liao T, Chen J, Xu Y (2019) Quality evaluation-based iterative seam estimation for image stitching. *Signal, Image and Video Processing* 13(6):1199–1206
- [18] Lin K, Jiang N, Cheong LF, et al (2016) Seagull: Seam-guided local alignment for parallax-tolerant image stitching. In: Proc. 14th Eur. Conf. Comput. Vision, pp 370–385
- [19] Lin WY, Liu L, Matsushita Y, et al (2012) Aligning images in the wild. In: IEEE Conference on Computer Vision and Pattern Recognition, pp 1–8
- [20] Liu C, Yuen J, Torralba A (2011) Sift flow: Dense correspondence across scenes and its applications. *IEEE Transactions on Pattern Analysis and Machine Intelligence* 33(5):978–994
- [21] Otsu N (1975) A threshold selection method from gray-level histograms. *Automatica* 11(285-296):23–27
- [22] Pérez P, Gangnet M, Blake A (2003) Poisson image editing. *ACM Trans Graph* 22(3):313–318
- [23] Szeliski R (2006) Image alignment and stitching: A tutorial. *Found Trends Comput Graph Vis* 2(1):1–104
- [24] Wang Z, Bovik AC, Sheikh HR, et al (2004) Image quality assessment: from error visibility to structural similarity. *IEEE Trans Image Processing* 13(4):600–612
- [25] Zaragoza J, Chin TJ, Tran QH, et al (2014) As-projective-as-possible image stitching with moving dlt. *IEEE Trans Pattern Anal Mach Intell* 7(36):1285–1298
- [26] Zhang F, Liu F (2014) Parallax-tolerant image stitching. In: Proc. IEEE Conf. Comput. Vision Pattern Recognit., pp 3262–3269
- [27] Zhang G, He Y, Chen W, et al (2016) Multi-viewpoint panorama construction with wide-baseline images. *IEEE Trans Image Processing* 25(7):3099–3111
- [28] Zhang L, Huang H (2022) Image stitching with manifold optimization. *IEEE Transactions on Multimedia* pp 1–1
- [29] Zhang Z, Yang X, Xu C (2021) Natural image stitching with layered warping constraint. *IEEE Transactions on Multimedia* pp 1–1
- [30] Zheng J, Wang Y, Wang H, et al (2019) A novel projective-consistent plane based image stitching method. *IEEE Transactions on Multimedia* 21(10):2561–2575

- [31] Zhu S, Zhang Y, Zhang J, et al (2023) Isgta: an effective approach for multi-image stitching based on gradual transformation matrix. *Signal, Image and Video Processing* pp 1–10